A Diffuse Reflectance Infrared Fourier-Transform Spectra and Density Functional Theory Study of CO Adsorption on Rh/γ-Al 2 O 3

ARTICLE *in* THE JOURNAL OF PHYSICAL CHEMISTRY C · SEPTEMBER 2007

Impact Factor: 4.77 · DOI: 10.1021/jp074549x

3 AUTHORS:

Constantinos D. Zeinalipour-Yazdi
University College London
30 PUBLICATIONS **291** CITATIONS

SEE PROFILE

Andrew L Cooksy
San Diego State University
63 PUBLICATIONS **1,395** CITATIONS

SEE PROFILE

Angelos M Efstathiou
University of Cyprus
137 PUBLICATIONS **3,328** CITATIONS

SEE PROFILE

A Diffuse Reflectance Infrared Fourier-Transform Spectra and Density Functional Theory Study of CO Adsorption on Rh/γ-Al_2O_3

Constantinos D. Zeinalipour-Yazdi,*,† Andrew L. Cooksy,‡ and Angelos M. Efstathiou*,†

Department of Chemistry, University of Cyprus, Nicosia, CY 1678, Cyprus, and Department of Chemistry, San Diego State University, San Diego, California 92122

Received: June 12, 2007; In Final Form: July 11, 2007

The vibrational frequencies and bond dissociation energies of carbon monoxide adsorbed to various rhodium clusters are computed, and the diffuse reflectance infrared Fourier-transform (DRIFT) spectrum of carbon monoxide adsorbed onto Rh/γ-Al_2O_3 is reported. The computations reveal that the spectral features that have previously been assigned to symmetric and antisymmetric vibrational modes of isolated dicarbonyl species on Rh can also be assigned to vibrational coupling of adjacent linearly bound carbonyl groups (atop M−CO). We explore, in small rhodium clusters, the effects of binding configuration, surface coverage, metal−support charge transfer, and cluster dimension on the vibrational frequency of the C−O bond and the adsorption energy of CO to rhodium. In particular, we find a linear correlation between the vibrational frequency of the carbon−oxygen bond with respect to the metal−carbonyl bond adsorption energy as well as the carbon-oxygen bond length for small rhodium clusters. A semiquantitative relationship is derived that may be used to calculate bond dissociation enthalpies of rhodium−carbonyl bonds with the use of crystallographic or IR data associated to the rhodium−carbonyl bond.

Introduction

Many commercial and industrial catalysts promote the reaction rate of chemical processes that involve the adsorption of carbon monoxide (CO) on supported-metal catalysts. Examples include the removal of CO from automobile exhaust emissions in the three-way catalytic converter[1] (TWC) or during the water−gas shift (WGS) reaction used to produce fuel-cell-compatible hydrogen.[2] Our interest in CO adsorption stems from our current effort to study the WGS reaction mechanism on highly dispersed Rh/γ-Al_2O_3 catalysts.[3] Thus, an important step toward the understanding of chemical reactions on Rh/γ-Al_2O_3 is to study the adsorption of CO onto small clusters that are present in highly dispersed catalysts.[4] Infrared (IR) spectroscopy has a long-standing history in the characterization of dispersed metals, and it has proven to be a powerful technique in studying the adsorption of CO onto various noble metal catalysts because of the sensitivity of the carbonyl vibrational frequency to the type of metal−carbonyl binding.[5,6] Dispersed noble metals such as Ru,[7] Rh,[8−11] Pd,[12−14] and Pt[15−19] supported on metal oxides have been extensively studied using transmission IR spectroscopy. These studies have led to the identification of various adsorbed CO species that are formed on the dispersed metal, as well as on the substrate[20] in some occasions. The assignment of spectral features is usually carried out by correlating the spectroscopic data obtained on metal-supported catalysts to metal−carbonyl compounds[21] and their dissociation products[22] or to single-crystal surfaces where the effects of coverage, isotopic exchange, and temperature evolution can be studied in a controlled fashion. Studies of this kind have provided valuable information about the various types of carbonyl groups that are formed on transition metals, such as linear (L-CO), bridge (B-CO), hollow (H-CO), dicarbonyl (di-CO) and tricarbonyl (tri-CO) species (see Figure 1).

These configurations of CO binding to the transition metals have been confirmed both by IR spectroscopy[8,11] and by high-resolution ^{13}C nuclear magnetic resonance (NMR) studies.[23,24] In particular, the IR spectroscopy studies with isotopic exchange and quantitative CO uptake measurements have revealed the existence of dicarbonyl species on isolated Rh^{+1} atoms, present in highly dispersed Rh/γ-Al_2O_3 catalysts.[11] Furthermore, the ^{13}C NMR studies showed that the L-CO:B-CO ratio is 1:1.5[24] and that B-CO is preferred to H-CO or higher metal coordinated carbonyls on Rh(111).[23] Multicarbonyl species such as dicarbonyls and tricarbonyls are also found on rhodium clusters, although the first are preferred in isolated rhodium atoms. Studies of the temperature evolution of the IR spectrum of adsorbed CO in Rh/γ-Al_2O_3 gave the sequence B-CO > L-CO > di-CO with respect to their thermal stability.[25] Furthermore, L-CO is "floppy" and undergoes a faster motion on rhodium than di-CO species that lie in a slower modulation regime, indicative of their isolated location on the substrate and suggestive of a low barrier for their diffusion.

The study of CO chemisorption onto single crystals of Rh[26,27] using IR spectroscopy has also revealed information about the adsorption mechanism and dynamics of CO diffusion. Furthermore, it has been shown that at high-coverage repulsive dipole−dipole interactions between adjacent CO groups may cause coupling of vibrational modes, splitting the band that corresponds to L-CO into a doublet.[28,29] More recently[30,31] the use of diffuse reflectance IR Fourier-transform spectroscopy (DRIFTS) has been employed to obtain in situ spectra of catalysts under reaction conditions. Here we obtain such a spectrum and carry out a spectral assignment based on the vibrational frequency trends obtained from quantum chemical calculations. Subsequently, we explore in small rhodium clusters the effects of

* Authors to whom correspondence should be addressed. E-mail: C.D.Z.: zeinalip@ucy.ac.cy; A.M.E.: efstath@ucy.ac.cy.
† University of Cyprus.
‡ San Diego State University.

10.1021/jp074549x CCC: $37.00
Published on Web 08/22/2007

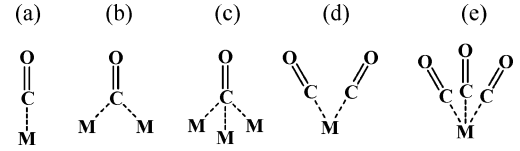

Figure 1. Schematic representation of the various $M_n-(CO)_m$ chemisorbed species reported in the literature. The commonly used nomenclature of the metal carbonyl species is (a) linear, (b) bridged, (c) hollow, (d) dicarbonyl, and (e) tricarbonyl.

binding configuration, surface coverage, metal−support electron transfer, and cluster dimension. Finally, a semiquantitative relationship is derived that could be used to calculate the Rh−CO bond dissociation enthalpy using crystallographic or IR data associated with the carbonyl bond.

Experimental Details

The catalyst, rhodium supported on γ-alumina (Rh/γ-Al_2O_3, 0.5% w/w) was prepared by the method of incipient wetness impregnation of γ-alumina (58 Å pore size, ~150 mesh, Aldrich) with an aqueous solution of the precursor compound, rhodium nitrate (10 w/w Rh in 5 wt % nitric acid, Aldrich). Under continuous stirring, we added 0.28 mL of the $Rh(NO_3)_3$ solution and 2 grams of γ-alumina to 100 mL of deionized water at room temperature. Subsequently, the water was evaporated at 120 °C for 12 h, and the resulting slurry was dried at 500 °C for 2 h. This was followed by a 2 h calcination in a 20% O_2/He gas mixture (50 cm^3/min) at 500 °C and a 2 h reduction in pure H_2 at 300 °C. It is noted that this catalyst preparation methodology results in catalysts with noble metal dispersions greater than 50%.[3]

DRIFTS were obtained on a Spectrum GX (Perkin Elmer) equipped with a DRIFTS cell (Harrick, Praying Mantis). A 1:5 ratio of the catalyst and dry KBr was finely powdered in a mortar and then placed into the sample holder. This ratio was found to give an improved signal-to-noise (S/N) ratio, which was further enhanced by exposing to the IR radiation a flat surface of the powder (through the use of a razor blade). The geometry of the KBr windows on the DRIFTS cell was such that the majority of the IR signal intensity was due to diffuse reflectance, rather than specular. The recorded DRIFTS signal was the reflected IR source energy after subtracting the DRIFTS spectrum of the solid catalyst in He flow (expressed in absorbance units). A volumetric flow rate of 50 cm^3/min and a composition of 2% CO/He under ambient conditions was used in all experiments. DRIFTS spectra were smoothed to remove high-frequency noise.

Computational Details

In this study we employed density functional theory calculations (DFT) as implemented in Gaussian 03,[32] with the use of the Becke's three-parameter hybrid exchange functional[33] combined with the Lee−Yang−Parr nonlocal correlation functional[34] (B3LYP). The basis set[35] used for rhodium (LanL2dz) is well suited for transition metals because it makes use of electron core potentials (ECP) to reduce computational demands without affecting the binding of the clusters that mostly involves the outer shell electrons. For carbon and oxygen, this basis set[36] was further augmented with one set of polarization functions, denoted as LanL2dz(pd). The coefficients[37] used for the polarization functions in carbon and oxygen were 0.587 and 0.961, respectively. Polarization was necessary to provide adequate variational flexibility of the one-electron wavefunctions

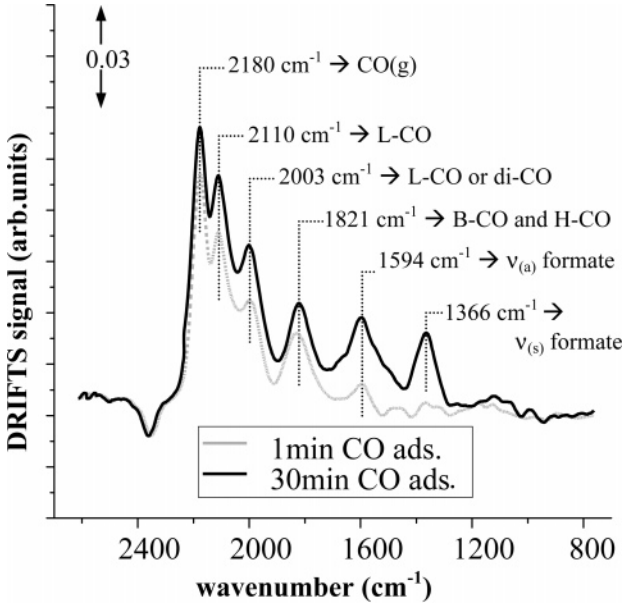

Figure 2. DRIFTS CO adsorption spectrum of 0.5 wt % Rh/γ-Al_2O_3 catalyst. Grey and black lines correspond to the DRIFTS spectrum taken after 1 and 30 min of 2% CO/He exposure, respectively.

that model the π-backdonation of the Rh−CO bond. Initially, the structures were optimized using the Hartree−Fock method with the smaller LanL2mb basis set.[38,39] The molecular geometry and wavefunctions were then used as an initial guess for the following optimizations. This optimization procedure, B3LYP/LanL2mb followed by B3LYP/LanL2dz(pd), was found to be critical for obtaining convergence of the molecular clusters studied. The Hessian was calculated analytically at every optimization step, and all structures were confirmed to be energetic minima on the potential energy surface by the absence of negative vibrational frequencies, unless otherwise mentioned. The self-consistent field convergence criteria for the root-mean-square (rms) density matrix and the total energy were set to 10^{-8} Hartrees/bohr and 10^{-6} Hartrees, respectively. Binding energies were corrected for basis set superposition error (BSSE) using the full counterpoise method by Boys and Bernardi.[40]

Results and Discussion

Experimental In Situ DRIFTS Studies. The catalyst used in the in situ DRIFTS studies, 0.5 wt % Rh/γ-Al_2O_3, had 53% metal dispersion.[3] A typical DRIFTS spectrum of this catalyst, exposed for 30 min to a 2% CO/He gas mixture at 50 cm^3/min volumetric flow rate under ambient conditions, can be seen in Figure 2. Spectra similar in intensity were obtained at even shorter CO exposure periods because time evolution of the peak intensities was observed only in the first minutes of the adsorption process. After that, a constant CO coverage was observed. Six adsorption bands are present in the DRIFTS spectrum. The assignment of these bands was carried out on the basis of the computationally derived vibrational frequencies.

The band positions shown were obtained by deconvolution of the DRIFTS spectrum with the use of six Gaussian-type functions ($R^2 = 0.998$). The intense band at 2180 cm^{-1} corresponds to the stretching vibrational mode of gas-phase CO.[41] The use of lower CO concentrations in the CO/He mixture showed a decrease of this adsorption band. The two subsequent, lower wavenumber bands were assigned to dicarbonyl species that are located on isolated Rh atoms.[8] However, as we demonstrate in the following sections, this doublet could also

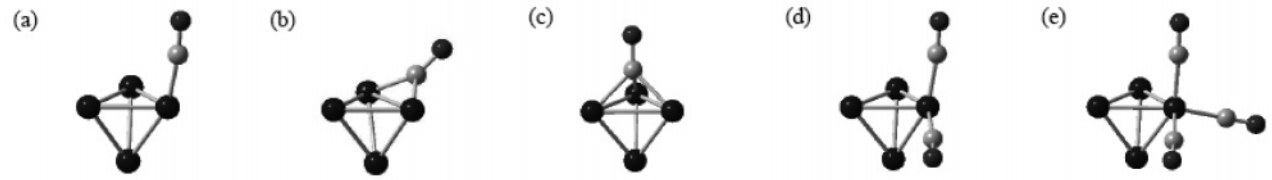

Figure 3. Optimized geometries at B3LYP/LanL2dz(pd) of various rhodium carbonyl clusters of the type $Rh_4(CO)_m$. In these rhodium clusters CO has a (a) linear, (b) bridge, (c) hollow, (d) dicarbonyl, and (e) tricarbonyl type configuration. Dark, medium, and light gray atoms correspond to rhodium, oxygen, and carbon, respectively.

correspond to the symmetric and antisymmetric stretching modes of coupled linear CO vibrations that appear when the surface coverage is greater than $^1/_3$ of a monolayer (ML). This phenomenon is not discussed in the literature for metal-supported catalysts, although it is known to occur on single crystals where extended two-dimensional (2D) terraces are available.[27,29,42] The broader band that follows at 1821 cm^{-1} is due to B-CO.[11] The two subsequent bands at 1594 cm^{-1} and 1366 cm^{-1}, having a slower rate of formation as indicated by their appearance only when the catalysts is exposed to CO for prolonged times, are the result of formate ion formation on the alumina support. In particular, these bands have previously been assigned to the antisymmetric ($\nu_{(a)} = 1595$ cm^{-1}) and symmetric ($\nu_{(s)} = 1380$ cm^{-1}) formate ion ($HCOO^-$) vibrations on γ-alumina.[43]

Theoretical DFT Studies. In this section, we employ high-level DFT computations to assign the various bands observed in the DRIFTS spectra. This was achieved by comparing the trends in vibrational frequency of CO in various types of metal carbonyl bonds (effect of binding site). The computations show a linear correlation between equilibrium C−O bond length and CO vibrational frequency and the M−CO bond adsorption energy and CO vibrational frequency. This correlation is used to derive semiquantitative relationships that correlate the three variables. Additionally, we study the effect of surface coverage and derive the zero-coverage bond dissociation enthalpy for linear rhodium−carbonyl moieties. Finally, the effect of metal−support charge transfer is explored as well as the effect of the cluster dimension on the vibrational bands that correspond to the C−O stretching in the IR spectrum.

i. Effect of the binding site. The effect of the binding site on the vibrational stretching frequency of the carbonyl group was studied by the examination of CO adsorption on a tetrahedral (T_d) rhodium cluster (Rh_4). The high unsaturation of the Rh atoms in these clusters offers the possibility for the formation of a wide variety of M−CO bonds. We have obtained BSSE corrected minima for the various adsorbed carbonyl species depicted in Figure 3, treating the rhodium cluster and the CO molecule as two fragments. These equilibrium configurations appear to have differences of less than a few thousandths of an angstrom in their bond lengths as compared to those of the non-BSSE optimized structures. Thus, in terms of the equilibrium structure, the BSSE correction had little effect. However, in terms of the calculated binding energies, its necessity becomes evident by comparing the BSSE-corrected and non-corrected bond adsorption energies in L-CO (−36.1 and −38.3 kcal/mol, respectively), B-CO (−62.5 and −49.1 kcal/mol, respectively), and H-CO (−52.2 and −39.2 kcal/mol, respectively). It is evident that an underestimation as large as 30% of the computed bond adsorption energy may occur if the Counterpoise correction method[40] is not applied to correct for the BSSE. The bridged binding of CO is the strongest among the various adsorption modes. It also causes the most drastic structural changes on Rh_4, because it leads to a partial disruption of the Rh−Rh bond at the position where CO is bound. Another consistent feature of these computations is that the metal−carbonyl bond weakens the Rh−Rh framework as well as the C−O bonds. This is seen by the general increase of the bond lengths in the $Rh_4(CO)_m$ complexes (Table 1) as compared to those of the isolated rhodium cluster and CO molecule. These results are reasonable because the Rh−CO bond dissociation energy (36.0 kcal/mol) is comparable to that of the Rh−Rh bond (32.5 kcal/mol).[44]

The vibrational coupling of the CO groups occurring in the di-CO moieties causes a frequency splitting of 43 cm^{-1} between symmetric and antisymmetric vibrational modes. This observation is in close agreement with gas-phase IR spectra of $Rh_2(CO)_4Cl_2$ that show a 42 cm^{-1} splitting.[45] The tri-CO species have a slightly higher (47 cm^{-1}) splitting with the antisymmetric, $\nu_{(a)}$(C═O), mode being twice as large in intensity as compared to the higher frequency symmetric stretch, $\nu_{(s)}$(C═O).

The trend in adsorption energy (A_o) of the various CO species present in $M_n-(CO)_m$ compounds is found to follow the order B-CO > H-CO > L-CO > di-CO > tri-CO. Yao et al.,[25] in IR thermal stability studies, found a similar sequence on a smaller set of binding configurations: B-CO > L-CO > di-CO. Furthermore, we calculate the IR- and Raman-active vibrational modes in these model clusters, and we obtain vibrational frequencies to compare to the experimental IR data obtained for Rh/γ-Al_2O_3. A linear correlation between the equilibrium C−O bond length (R_{CO}) and the vibrational frequency of the C−O stretching (ν_{CO}) is demonstrated in Figure 4a. Linear regression ($R^2 = 0.999$) yields the following relationship (eq 1);

$$R_{CO}\,(\text{Å}) = (-1.493\times10^{-4})\nu_{CO}\,(\text{cm}^{-1}) + 1.4687 \quad (1)$$

which may be used to estimate the vibrational stretching frequency of CO groups in rhodium−carbonyl compounds for which crystallographic data are available. Furthermore, we obtained a near-linear correlation between the adsorption energy of CO on rhodium and the C−O vibrational stretching frequency, as shown in Figure 4b. In particular, the sequence of vibrational frequencies of the carbonyl groups is the reverse of the sequence of bond dissociation energies. The adsorption energy of CO to Rh_4 does not follow this linear trend, and we attribute this to the unique nature of this bond, which significantly disrupts the Rh−Rh framework. In particular, the Rh−Rh bond length adjacent to the carbonyl group is found to be 2.962, 2.733, and 2.545 Å (average of three Rh−Rh bonds) for B-CO, H-CO and L-CO, respectively. Linear regression ($R^2 = 0.999$) in which the B-CO datapoint is omitted yields eq 2;

$$A_o\,(\text{kcal/mol}) = 0.053033\nu_{CO}\,(\text{cm}^{-1}) - 143.445 \quad (2)$$

where A_o is the adsorption energy of CO to rhodium. A combination of eqs 1 and 2 results in a semiquantitative equation

TABLE 1: Binding Strength, IR/Raman Vibrational Frequencies, Normalized Peak Intensities, and Bond Lengths of Various $Rh_4(CO)_m$ (m = 1,2,3) Clusters That Are Representative of the Different Adsorption Modes of CO to Tetrahedral Rhodium Clusters

				theoretical		experimental		
species	point group	A_o[a] (kcal/mol)	vibrational modes	ν_{IR} (I_{IR})[b] (cm^{-1})	ν_{Raman} (I_{Raman}) (cm^{-1})	ν_{IR} (cm^{-1})	ref	bond length[c] (Å)
CO(g)	$D_{\infty}h$	n/a	s(C═O)	2182 (100%)	2182 (100%)	2180	this work	1.143
Rh_4	T_d	n/a	s(Rh−Rh)		317 (100%)			2.496
L-CO	C_s	−36.1 (−38.3)[d]	s(C═O) s(Rh−C) s(Rh−Rh)	2030 (100%)	2030 (75%) 462 (6%) 304 (19%)	2040	9	1.164 1.885 [2.518]
B-CO	C_s	−62.5 (−49.1)	s(C═O) s(Rh−C) s(Rh−Rh)	1761 (100%)	1761 (71%) 437 (17%) 290 (12%)	1821	this work	1.206 1.921 [2.598]
H-CO	C_{3v}	−52.2 (−39.2)	s(C═O) anti-s(Rh−C) sym-s(Rh−C) s(Rh−Rh)	1706 (100%)	1706 (60%) 441 (15%) 425 (15%) 277 (10%)	n/a		1.214 2.012 [2.609]
di-CO	C_s	−33.3	sym-s(C═O) anti-s(C═O) s(Rh−C) s(Rh−Rh)	2082 (50%) 2039 (50%)	2082 (22%) 2039 (69%) 298 (9%)	2100 2030	11 11	1.158 1.926 [2.598]
tri-CO	C_{3v}	−31.1	sym-s(C═O) anti-s(C═O) s(Rh−C) s(Rh−Rh)	2109 (33%) 2062 (67%)	2109 (5%) 2062 (82%) 301 (13%)	n/a n/a		1.155 1.955 [2.540]

[a] BSSE corrected adsorption energy (A_o) of CO to rhodium cluster, given by $E(Rh_4) + mE(CO) - E(Rh_4(CO)_m)$ where each energy is computed using the full basis of the rhodium−carbonyl cluster $Rh_4(CO)_m$. [b] Infrared and Raman intensities are normalized to the highest intensity peak. Intensities lower than 5% of the highest intensity peak are not accounted.

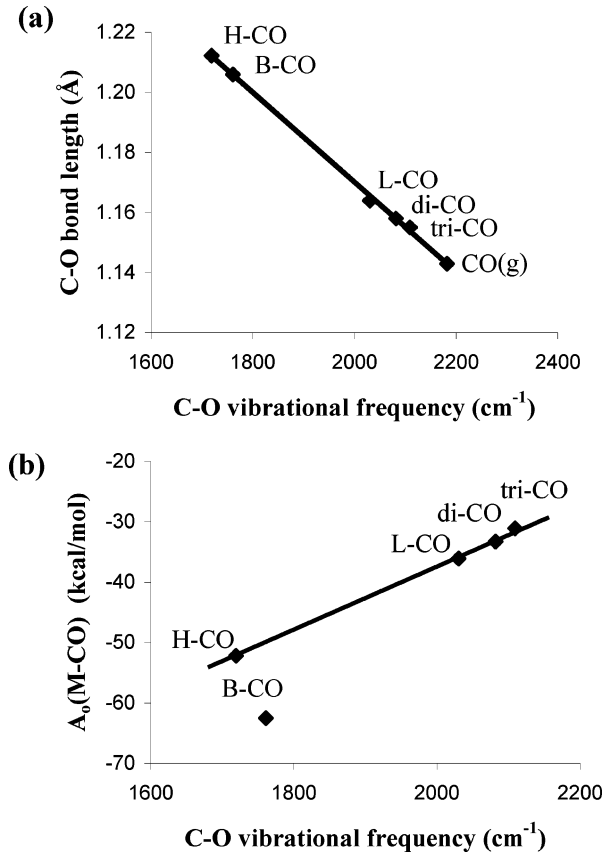

Figure 4. Graph showing linear correlation between (a) the equilibrium C−O bond length and CO vibrational frequency and (b) the M−CO adsorption energy and CO vibrational frequency in the various types of CO adsorbed species found on tetrahedral Rh_4 clusters.

that can estimate the adsorption energy of any type of Rh−CO bond with the use of crystallographically-derived bond lengths. This relationship is given by eq 3, and it should yield binding energies to an accuracy of ± 1 kcal/mol.

$$A_o\ (\text{kcal/mole}) = -3.5521\times10^2(R_{CO}(\text{Å}) - 1.4687) - 143.445 \quad (3)$$

ii. Effect of Surface Coverage. The adsorption energy on transition metal surfaces increases linearly with surface coverage (θ) when interactions between adsorbed species are small. However, this does not occur in the case of CO, where the presence of a dipole moment (0.112 D, 3.74×10^{-31} C m) and the parallel configuration on flat terraces, such as the (111) or the (100), causes repulsive interactions that scale as $1/d^3$, where d is the distance between the interacting CO molecules.[46] Thus, it is reasonable to expect that, at high surface coverages, enhancement of the dipole−dipole repulsions will weaken the M−CO bond. This has repeatedly been observed in thermal desorption studies of CO from Rh(111) and Rh(100) surfaces, in which a −50 °C shift in the desorption temperature is observed as CO exposure is increased.[47] Furthermore, it is well-known that this also affects the C−O stretching frequency.[27] To see if our model cluster would show a similar decrease of the CO binding energy, we increased the number of CO groups adsorbed on one face of the molecular cluster. Figure 5 shows that there is a near-linear correlation between the surface coverage and A_o for small rhodium clusters. The zero-coverage bond dissociation enthalpy of CO to small rhodium clusters (38.8 kcal/mol) is found to be in excellent agreement with the experimental value (39.4 kcal/mol) obtained from thermal desorption spectroscopy studies.[48] The IR vibrational frequencies and the molecular configurations from these computations are tabulated in Table 2. Once the surface coverage exceeds $^1/_3$ of a monolayer, a second lower wavenumber vibrational band appears that results from vibrational coupling between the adjacent L-CO groups. The two vibrational modes, symmetric

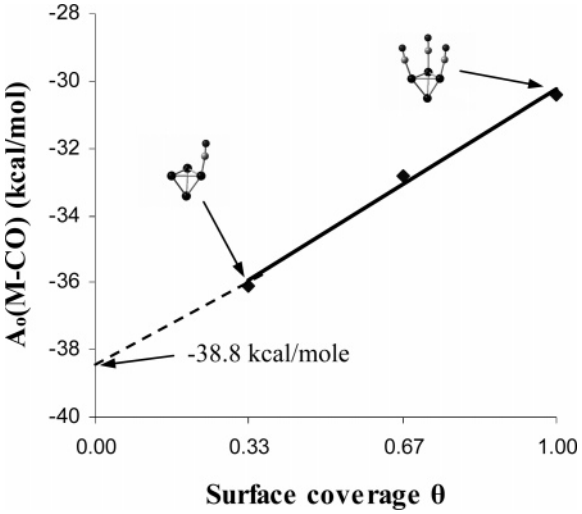

Figure 5. Graph showing linear correlation of CO adsorption energy (A_o) and CO surface coverage (θ_{CO}) on T_d Rh_4 clusters. Note that we assume that CO can bind only to one out of the four faces of the cluster. Dark, medium, and light gray atoms correspond to rhodium, oxygen and carbon, respectively.

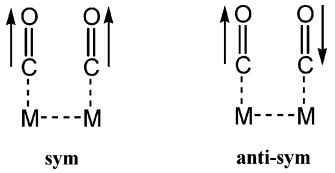

Figure 6. Simplified schematic of vibrational coupling between L-CO groups at high surface coverage.

(sym) and antisymmetric (anti-sym), that emerge from the vibrational coupling between L-CO groups are depicted in Figure 6. To the best of our knowledge, the existence of such vibrational coupling on small metal clusters has not been previously reported.

iii. Effect of Metal−Support Charge Transfer. Changes to the catalytic activity of highly dispersed metal-supported catalysts are often attributed to charge transfer between metal and support.[49] An increase of the support alkalinity causes an increase of the electron density located at the oxygen sites in metal oxides, resulting in electron transfer from the support to the metal particle.[50,51] Likely, delocalized support surface hydroxyl groups (−OH) and oxygen anions (O^{n-}) that interact with the metal particles can withdraw electron density from the metal particle, generating a positive charge on the metal nanoparticles.[52] Computationally, charge-transfer effects can be easily modeled by introducing negative or positive charges to the metal−CO cluster. This way, we implicitly monitor the effect that metal−support charge transfer would have on the binding of CO due to the electron-donating or -withdrawing character of the support material. The effect of metal−support charge transfer onto the vibrational stretching frequency of the carbonyl group can be seen in Figure 7. It is obvious that electron donating substrates will reduce the vibrational stretching frequency of the CO groups, suggestive of the stronger rhodium−carbonyl bond strength shown in section (i). In contrast, electron-withdrawing substrates will have the reverse effect. In particular, our computations indicate a near-linear relationship between metal cluster charge and the carbonyl vibrational frequency, which is attributed to charge transfer of additional electron density located at the metal through π-back-donation to the $2\pi^*$ orbital of the CO moiety.[53] The greater is the metal cluster negative charge, the stronger the M−CO bond and, consequently, the lower the vibrational stretching frequency of C−O bond. These computational results are in agreement with recent time-of-flight mass spectrometry (TOFMS) experiments on molecular beams of anionic, neutral, and cationic rhodium cluster-CO complexes. Infrared spectroscopy in those experiments showed a linear relationship between the cluster charge and ν(CO) for $Rh_nCO^{-/0/+}$ over the size range n = 3−15.[54,55] The $Rh_4(CO)_3^{2+}$ cluster appears to have a nonclassical behavior for the CO vibration, with stretching frequencies $\nu_{(s)}$ = 2227 cm^{-1} and $\nu_{(a)}$ = 2201 cm^{-1} both exceeding that of gas-phase CO (ν = 2182 cm^{-1}). This phenomenon is known and has previously been attributed to an electrostatic effect caused between the positive charge of the metal cluster and the polarized $C^{\delta+}-O^{\delta-}$ bond. The net result is a shift in charge from the oxygen toward the carbon, increasing the covalency of the C−O bond.[56,57]

iv. Effect of Cluster Dimensions. The simulated IR spectra of two trigonal-pyramidal rhodium−carbonyl clusters, Rh_4-(3,1)−$(CO)_3$ and Rh_{10}(6, 3, 1)−$(CO)_6$, are presented first to confirm the existence of the vibrational coupling between linear carbonyl groups (L-CO) in extended (111) surfaces (at high θ), and second to obtain the dependence of the sym and anti-sym vibrational stretching frequency bands as a function of rhodium cluster dimension. The atomic positions of rhodium atoms were

TABLE 2: M−CO Adsorption Energy, Infrared and Raman Vibrational Frequencies, and Bond Lengths of Various Representative $Rh_4(CO)_m$ (m = 1,2,3) Clusters as a Function of Surface Coverage (θ_{CO})

					theoretical		
species	point group	A_o[a] (kcal/mol)	θ_{CO}[b]	vibrational modes	ν_{IR} (cm^{-1})	ν_{Raman} (cm^{-1})	bond length[c] (Å)
CO	$D_{\infty}h$	n/a	n/a	s(C═O)	2182(s)	2182(s)	1.143
Rh_4	T_d	n/a	n/a	s(Rh−Rh)		317(s)	2.496
Rh_4−L-CO	C_s	−36.1	0.33	s(C═O)	2030(s)	2030(s)	1.164
		(−38.3)[d]		s(Rh−C)		462(w)	1.885
				s(Rh−Rh)		304(w)	[2.518]
Rh_4−$(L\text{-}CO)_2$	C_s	−32.8	0.67	sym s(C═O)	2063(s)	2063(m)	1.160
		(−35.2)		anti s(C═O)[d]	2023(m)	2023(s)	
				s(Rh−C)		435(vw)	1.916
				s(Rh−Rh)		293(w)	[2.529]
Rh_4−$(L\text{-}CO)_3$	C_{3v}	−30.4	1.00	sym s(C═O)	2089(s)	2089(m)	1.158
		(−33.2)		anti s(C═O)[d]	2035(m)	2035(s)	
				s(Rh−C)		444(vw)	1.941
				s(Rh−C)		415(vw)	
				s(Rh−Rh)		283(m)	[2.535]

[a] Adsorption energy (A_o) of CO to rhodium cluster, given by $E(Rh_4) + mE(CO) - E(Rh_4(CO)_m)$ [b] Coverage is $\theta_{CO} = n(CO)/n(Rh)$, where n(CO) and n(Rh) the number of surface CO molecules and rhodium atoms, respectively. [c] The Rh−Rh bond length was taken as the average bond length.

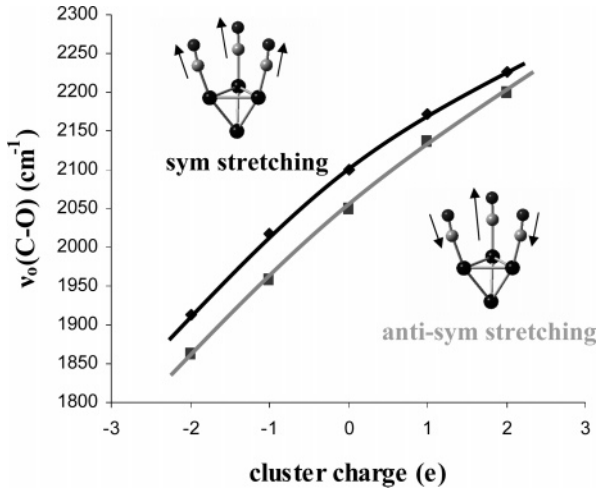

Figure 7. Graph showing near-linear correlation between CO vibrational frequency and rhodium cluster charge at high surface coverage. Note that only one of the two anti-sym stretching modes is shown. Dark, medium, and light gray atoms correspond to rhodium, oxygen, and carbon, respectively.

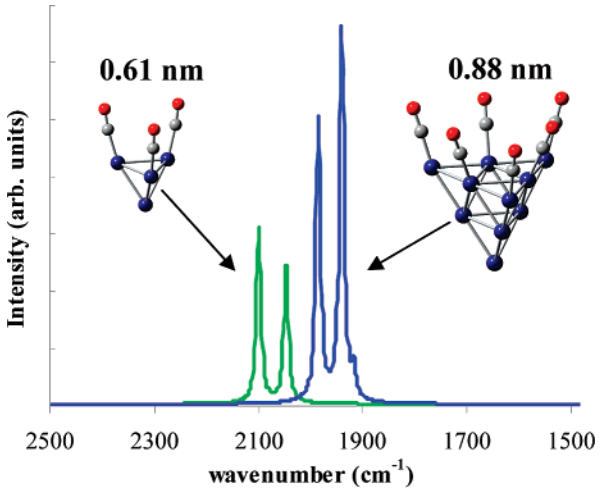

Figure 8. Simulated IR spectra of adsorbed CO on rhodium clusters at high θ_{CO}. The spectra show the existence of vibrational coupling between L-CO groups on the (111) surface. Cluster dimension (d) is defined as the sum of the distances between two corner rhodium atoms plus two rhodium atomic radii (173 pm).[59]

fixed to those of bulk rhodium[58] using a cubic close-packed unit cell with a lattice constant of $a = 3.8034$ Å ($R_{Rh-Rh} = 2.6894$ Å). This treatment, rather than full optimization, resulted in a few negative vibrational frequencies in relation to the Rh_{10}-(6, 3, 1) vibrations. However, these appear to have very little coupling to the CO vibrations and thus are not expected to alter the IR spectra significantly. The L-CO groups were initially positioned directly over rhodium atoms, at a 90° angle with respect to the (111) crystallographic cluster plane, and were subsequently allowed to relax without any additional constraints. A significant advantage of these two clusters with respect to other possible cluster geometries is the even number of rhodium atoms present. This results in a close-shell electronic configuration, which can be treated with the computationally more efficient restricted B3LYP method (RB3LYP). Furthermore, the high-symmetry point group C_{3v} further reduces the computational expense.

The simulated infrared spectra (Figure 8) clearly demonstrate the existence of a vibrational coupling between L-CO groups on larger (111) surfaces of the rhodium clusters, indicated by the appearance of two adsorption bands. In particular, the higher-frequency band corresponds to the cooperative sym stretching of all L-CO groups at the surface, whereas the lower-frequency band corresponds to a superposition of $n-1$ anti-sym vibrational modes (n = number of L-CO groups). The L-CO groups are not entirely parallel, indicative of the repulsive interaction between parallel CO groups or a possible edge effect due to the finite size of the cluster. The same bands had previously been attributed to sym (2101 cm^{-1}) and anti-sym (2031 cm^{-1}) stretching in dicarbonyl species.[8,9] Here we show that vibrational coupling between linear CO species (L-CO), at high surface coverage of CO, may cause the appearance of the two bands. Thus, care should be taken in derivation of the chemical structure of adsorbed surface CO active species from DRIFTS steady-state isotopic transient kinetic analysis (SSITKA) data, with respect to reaction mechanisms occurring on metal-supported catalysts.[3]

It is evident that an increase of the rhodium cluster dimensions causes a dramatic downward shift of the C−O vibrational stretching frequency. In particular, a red-shift of 116 and 104 cm^{-1} occurs in the sym (higher wavenumber) and anti-sym stretching frequencies, respectively, when the cluster dimensions are increased by only 20%. However, the wavenumber difference between the sym and anti-sym stretching modes remains roughly constant at $\Delta\upsilon = 52$ and 44 cm^{-1} for $Rh_4(3,1)-(CO)_3$ and $Rh_{10}(6, 3, 1)-(CO)_6$, respectively.

The lower vibrational frequencies observed in larger rhodium carbonyl clusters are suggestive of stronger M−CO bonds, as shown in section (i). This can be attributed to the enhanced π-backdonation due to the greater polarizability of larger rhodium clusters. As a consequence, when the rate-determining step of a heterogeneously catalyzed reaction involves M−CO bond breaking, then high dispersion of the metal would be preferred to enhance the catalyst's activity.

Conclusions

The adsorption of CO to rhodium clusters was studied by employing DFT computations. On the basis of these results, the assignment of a DRIFTS spectrum of highly dispersed Rh/γ-Al_2O_3 exposed to CO is obtained. Surprisingly, certain spectral bands found in DRIFTS spectra of this catalyst, previously assigned to anti-sym and sym vibrational modes of isolated dicarbonyl species (di-CO), can also be assigned to vibrational coupling between adjacent L-CO groups.

Furthermore, several linear or near-linear relationships concerning the M−CO binding were derived which correlate: (a) the carbonyl bond length (R_{CO}) to the vibrational stretching frequency (ν_{CO}) of the carbonyl group, (b) the CO adsorption energy (A_o) to the vibrational stretching frequency (ν_{CO}) of the carbonyl group, (c) the CO adsorption energy (A_o) to the surface coverage of CO (θ_{CO}), and (d) the vibrational stretching frequency (ν_{CO}) of the carbonyl group to the net charge of the cluster.

Finally, semiquantitative relationships are derived that may be used to calculate bond dissociation enthalpies of rhodium−carbonyl bonds with the use of crystallographic or IR data associated to the bond.

Acknowledgment. The Cyprus Research Promotion (CRP) Foundation is acknowledged for financially supporting this project under the grant ΠΕΝΕΚ ΕΝΙΣΧ/0506/62. The Computational Science Research Center (CSRC) is acknowledged for their partial contribution of computer resources.

Supporting Information Available: Cartesian coordinates of the rhodium carbonyl clusters used in this work are available via the Internet at http://pubs.acs.org.

References and Notes

(1) Emrah, O.; Christian, H.; Goodman, D. W. *Top. Catal.* **2004**, *28*, 13.
(2) Faur Ghenciu, A. *Cur. Opin. Sol. State Mat. Sci.* **2002**, *6*, 389.
(3) Olympiou, G. G.; Kalamaras, C. M.; Zeinalipour, C. D.; Efstathiou, A. M. *Catal. Today* **2007**, *in press*.
(4) Estiu, G. L.; Zerner, M. C. *J. Phys. Chem.* **1993**, *97*, 13720.
(5) Little, L. H. *Infrared Spectra of Adsorbed Species*; Academic: London, 1966.
(6) Hair, M. L. *Infrared Spectroscopy in Surface Chemistry*; Marcel Dekker: New York, 1967.
(7) King, D. L. *J. Catal.* **1980**, *61*, 77.
(8) Yates, J. T., Jr.; Duncan, T. M.; Worley, S. D.; Vaughan, R. W. *J. Chem. Phys.* **1979**, *70*, 1219.
(9) Yang, A. C.; Garland, C. W. *J. Chem. Phys.* **1957**, *61*, 1504.
(10) Trautmann, S.; Baerns, M. *J. Catal.* **1994**, *150*, 335.
(11) Cavanagh, R. R.; Yates, J. T., Jr. *J. Chem. Phys.* **1981**, *74*, 4150.
(12) Tiznado, H.; Fuentes, S.; Zaera, F. *Langmuir* **2004**, *20*, 10490.
(13) Tessier, D.; Rakai, A.; Bozon-Verduraz, F. *J. Chem. Soc., Farad. Trans.* **1992**, *88*, 741.
(14) Yates, Jr., J. T.; Gelin, P.; Beebe, T. P., Jr. *IR Spectroscopic Characterization of Adsorbed Species and Processes on Surfaces*; Division of Colloid and Surface Chemistry, American Chemical Society: Philadelphia, Pennsylvania, 1984; Vol. August.
(15) Anderson, J. A. *J. Catal.* **1993**, *142*, 153.
(16) Barth, R.; Pitchai, R.; Anderson, R. L.; Verykios, X. E. *J. Catal.* **1989**, *116*, 61.
(17) Bourane, A.; Bianchi, D. *J. Catal.* **2003**, *218*, 447.
(18) Bourane, A.; Dulaurent, O.; Bianchi, D. *J. Catal.* **2000**, *196*, 115.
(19) Ferri, D.; Bürgi, T.; Baiker, A. *Phys. Chem. Chem. Phys.* **2002**, *4*, 2667.
(20) Zecchina, A.; Platero, E. E.; Areàn, C. O. *J. Catal.* **1987**, *107*, 244.
(21) Yang, A. C.; Garland, C. W. *J. Phys. Chem.* **1957**, *61*, 1504.
(22) Smith, A. K.; Hugues, F.; Theolier, A.; Basset, J. M.; Ugo, R.; Zanderighi, G. M.; Bilhou, J. L.; Graydon, W. F. *Inorg. Chem.* **1979**, *18*, 3104.
(23) Duncan, T. M.; Zilm, K. W.; Hamilton, D. M.; Root, T. W. *J. Phys. Chem.* **1989**, *93*, 2583.
(24) Duncan, T. M.; Root, T. W. *J. Phys. Chem.* **1988**, *92*, 4426.
(25) Yao, H. C.; Rothschild, W. G. *J. Chem. Phys.* **1978**, *68*, 4774.
(26) Pancír, J.; Haslingerová, I. *Czech. J. Phys.* **1989**, *39*, 1392.
(27) Xu, J.; Yates, J. T., Jr. *Surf. Sci.* **1995**, *327*, 193.
(28) Severson, M. W.; Stuhlmann, C.; Villegas, I.; Weaver, M. J. *J. Chem. Phys.* **1995**, *103*, 9832.
(29) Persson, B. N. J.; Ryberg, R. *Phys. Rev. B* **1981**, *24*, 6954.
(30) Tibiletti, D.; Goguet, A.; Reid, D.; Meunier, F. C.; Burch, R. *Catal. Today* **2006**, *113*, 94.
(31) Goguet, A.; Meunier, F. C.; Tibiletti, D.; Breen, J. P.; Burch, R. *J. Phys. Chem. B* **2004**, *108*, 20240.
(32) Frisch, M. J.; Trucks, G. W.; Schlegel, H. B.; Scuseria, G. E.; Robb, M. A.; Cheeseman, J. R.; Montgomery, J. A., Jr.; Vreven, T.; Kudin, K. N.; Burant, J. C.; Millam, J. M.; Iyengar, S. S.; Tomasi, J.; Barone, V.; Mennucci, B.; Cossi, M.; Scalmani, G.; Rega, N.; Petersson, G. A.; Nakatsuji, H.; Hada, M.; Ehara, M.; Toyota, K.; Fukuda, R.; Hasegawa, J.; Ishida, M.; Nakajima, T.; Honda, Y.; Kitao, O.; Nakai, H.; Klene, M.; Li, X.; Knox, J. E.; Hratchian, H. P.; Cross, J. B.; Adamo, C.; Jaramillo, J.; Gomperts, R.; Stratmann, R. E.; Yazyev, O.; Austin, A. J.; Cammi, R.; Pomelli, C.; Ochterski, J. W.; Ayala, P. Y.; Morokuma, K.; Voth, G. A.; Salvador, P.; Dannenberg, J. J.; Zakrzewski, V. G.; Dapprich, S.; Daniels, A. D.; Strain, M. C.; Farkas, O.; Malick, D. K.; Rabuck, A. D.; Raghavachari, K.; Foresman, J. B.; Ortiz, J. V.; Cui, Q.; Baboul, A. G.; Clifford, S.; Cioslowski, J.; Stefanov, B. B.; Liu, G.; Liashenko, A.; Piskorz, P.; Komaromi, I.; Martin, R. L.; Fox, D. J.; Keith, T.; Al-Laham, M. A.; Peng, C. Y.; Nanayakkara, A.; Challacombe, M.; Gill, P. M. W.; Johnson, B.; Chen, W.; Wong, M. W.; Gonzalez, C.; Pople, J. A. *Gaussian 0*3; Gaussian Inc.: Pittsburgh, Pennsylvania, 2003.
(33) Becke, A. D. *J. Chem. Phys.* **1993**, *98*, 5648.
(34) Lee, C.; Yang, W.; Parr, R. G. *Phys. Rev. B* **1988**, *37*, 785.
(35) Hay, P. J.; Wadt, W. R. *J. Chem. Phys.* **1985**, *82*, 270.
(36) Dunning, T. H., Jr.; Hay, P. J. *Modern Theoretical Chemistry*; Plenum: New York, 1976; Vol. 3.
(37) Check, C. E.; Faust, T. O.; Bailey, J. M.; Wright, B. J.; Gilbert, T. M.; Sunderlin, L. S. *J. Phys. Chem. A* **2001**, *105*, 8111.
(38) Collins, J. B.; Schleyer, P. V. R.; Binkley, J. S.; Pople, J. A. *J. Chem. Phys.* **1976**, *64*, 5142.
(39) Hehre, W. J.; Stewart, R. F.; Pople, J. A. *J. Chem. Phys.* **1969**, *51*, 2657.
(40) Boys, S. F.; Bernardi, F. *Mol. Phys.* **1970**, *19*, 553.
(41) Yates, J. T., Jr.; Gelin, P.; Beebe, T. P., Jr. *IR Spectroscopic Characterization of Adsorbed Species and Processes on Surfaces*; Division of Colloid and Surface Chemistry, American Chemical Society: Philadelphia, Pennsylvania, 1984; Vol. August.
(42) Greenler, R. G.; Leibsle, F. M.; Sorbello, R. S. *Phys. Rev. B* **1985**, *32*, 8431.
(43) Busca, G.; Lamotte, J.; Lavalley, J. C.; Lorenzelli, V. *J. Am. Chem. Soc.* **1987**, *109*, 5197.
(44) Bar, G. *Pure Appl. Chem.* **1986**, *58*, 543.
(45) Garland, C. W.; Wilt, J. R. *J. Chem. Phys.* **1962**, *36*, 1094.
(46) Atkins, P. W.; Friedman, R. S. *Molecular Quantum Mechanics*, 3rd ed.; Oxford University Press: Oxford, 1997.
(47) Castner, D. G.; Sexton, B. A.; Somorjai, G. A. *Surf. Sci.* **1978**, *71*, 519.
(48) Smedh, H. A. B.; Borg, M.; Nyholm, R.; Andersen, J. N. *Surf. Sci.* **2001**, *115*, 491.
(49) Ioannides, T.; Verykios, X. E. *J. Catal.* **1996**, *161*, 560.
(50) Sugimoto, M.; Katsuno, H.; Hayasaka, T.; Ishikawa, N.; Hirasawa, K. *Appl. Catal. A* **1993**, *102*, 167.
(51) de Mallmann, A.; Barthomeuf, D. *J. Chim. Phys.* **1990**, *87*, 535.
(52) Larsen, G.; Haller, G. L. *Catal. Lett.* **1989**, *3*, 103.
(53) Blyholder, G. *J. Phys. Chem. B* **1964**, *68*, 2772.
(54) Fielicke, A.; von Helden, G.; Meijer, G.; Pedersen, D. B.; Simard, B.; Rayner, D. M. *J. Phys. Chem. B* **2004**, *108*, 14591.
(55) Fielicke, A.; Helden, G. V.; Meijer, G.; Simard, B.; Dénommée, S.; Rayner, D. M. *J. Am. Chem. Soc.* **2003**, *125*, 11184.
(56) Lupinetti, A. J.; Fau, S.; Frenking, G.; Strauss, S. H. *J. Phys. Chem. A* **1997**, *101*, 9551.
(57) Goldman, A. S.; Krough-Jespersen, K. *J. Am. Chem. Soc.* **1996**, *118*, 12159.
(58) Singh, H. P. *Acta Crystallogr. A* **1968**, *24*, 469.
(59) Clementi, E.; Raimondi, D. L.; Reinhardt, W. P. *J. Chem. Phys.* **1963**, *38*, 2686.